Tailoring Ultrasound-Induced Growth of Perylene Diimide Nanowire Crystals from Solution by Modification with Poly(3-hexyl thiophene)

Laju Bu,[†,‡] Trenton J. Dawson,[†] and Ryan C. Hayward*[,†]

[†]Department of Polymer Science and Engineering, University of Massachusetts, Amherst, Massachusetts 01003, United States and [‡]School of Science, University of Xi'an Jiaotong University, Xi'an, Shaanxi 710049, P.R. China

ABSTRACT Tailoring nanocrystalline morphologies of organic semiconductors holds importance for organic electronics due to the influence of crystal characteristics on optoelectronic properties. Soluble additives that control crystal growth are commonly found in a variety of contexts such as biomineralization, pharmaceutical processing, and food science, while the use of ultrasound to modify crystal nucleation and growth has been routinely employed in producing crystals of food ingredients, biomolecules, pharmaceuticals, and inorganic materials. However, both methods have been applied to the growth of organic semiconductor crystals only in limited fashion. Here, we combine these two approaches to show that colloidally stable nanowire suspensions of a n-type small molecule, perylene diimide (PDI), can be prepared with well-controlled structures by sonocrystallization in the presence of a p-type polymer, poly(3-hexyl thiophene) (P3HT), as a soluble additive. By preferentially adsorbing on lateral crystal faces, P3HT dramatically reduces PDI crystal growth rate in the lateral directions relative to that along the nanowire axis, yielding nanocrystals with widths below 20 nm and narrow width distributions. With the use of uniform short PDI nanowires as seeds and extension with metastable solutions, controlled growth of PDI nanowires by "living crystallization" is demonstrated, providing access to narrowed length distributions and tailored branched crystal morphologies.

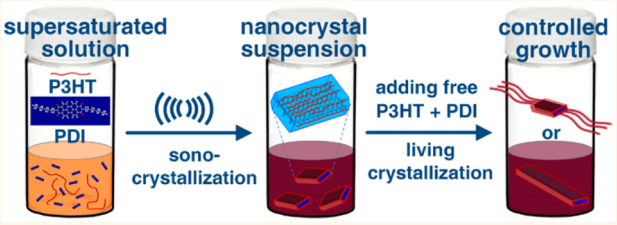

KEYWORDS: organic nanocrystals · soluble additive · selective adsorption · sonocrystallization · seeded crystallization · living crystallization

The degree of crystallinity and the size and shape of crystals play vital roles in optoelectronic applications of organic semiconductors due to the structure-dependent absorption, charge separation, and charge transport properties of these materials.[1−3] For example, in the case of organic photovoltaic devices, numerous methods have been developed to control crystallization of organic semiconductors, including thermal and solvent vapor annealing of thin films, addition of low-volatility components or marginal solvents to induce crystallization in solution or during film casting, and modifications to chemical structure that facilitate molecular packing.[4−7] The formation of controlled crystalline nanostuctures in solution prior to casting of device layers is attractive since it is amenable to incorporation into low-cost, large-scale processing approaches (*e.g.*, roll-to-roll fabrication), and can potentially eliminate the need for sensitive annealing steps after casting.[8]

Precrystallization of conjugated polymers in the form of nanofibers or nanoparticles,[9,10] starting from the most widely studied model p-type polymers, poly(3-alkyl thiophene)s (P3ATs), has been realized *via* recrystallization by cooling solutions in marginal solvents to induce supersaturation,[11,12] by adding a poor solvent to a solution in a good solvent,[13,14] or by a miniemulsion process.[15,16] Nanofibers obtained in this fashion are usually ∼10−20 nm wide, and can remain stably suspended for long periods of time, as has also been demonstrated for P3AT block copolymers,[17] low band gap polymers,[18] and n-type polymers.[19] By contrast, most small molecule organic semiconductors—such as naphthalene diimides,[20] perylene diimides[21,22] and acenes[23]—have limited

* Address correspondence to hayward@umass.edu.

Received for review November 28, 2014 and accepted February 5, 2015.

Published online February 10, 2015
10.1021/nn506795q

solubility in common organic solvents and exhibit rapid crystallization into micrometer-scale crystals that easily precipitate from solution. For this reason, there have so far been few reports on the preparation of stable suspensions of small molecule semiconductor nanocrystals.[24] Perylene diimide derivatives are of particular interest in this respect, since recent studies have shown that controlling their packing can greatly promote performance in photovoltaic devices.[25]

Recently, we reported that mixtures of poly(3-hexyl thiophene) (P3HT) with n-type perylene diimide (PDI) derivatives form shish-kebab-like p/n heterostructures upon casting from solution.[26] We suggested that this behavior depends upon the ability of P3HT to act as a "soluble additive" during growth of PDI crystals by adsorbing preferentially on certain crystal faces, thereby slowing lateral growth relative to longitudinal growth and yielding extended one-dimensional PDI nanowires. These PDI nanowires subsequently serve as efficient nucleation sites to induce crystallization of P3HT nanofibers that grow orthogonal to the PDI wire axis. Similar shish-kebab heterostuctures have been measured by Li *et al.* to exhibit anomalously high open circuit voltages for single-nanostructure photovoltaic devices, an effect attributed to the large interfacial area between P3HT and PDI.[27] The use of P3HT as a soluble additive has subsequently been extended to modify crystallization of other conjugated small molecules. In one case, Chen *et al.* found that P3HT, as well as a pentacene–bithiophene copolymer, can not only influence crystal size, but also alter the crystal polymorph adopted by 6,13-bis(triisopropylsilylethynyl) pentacene, yielding previously unreported crystal structures with excellent long-range order and improved charge transport.[28] In another, Suzuki *et al.* prepared nanowires of a tetracene derivative in the presence of P3HT which showed changes in morphology due to modification by the conjugated polymer, along with improvements in photoconductivity.[29]

Soluble additives that control crystallization through interactions with solutes to promote or retard crystal nucleation or growth, or to modulate crystalline polymorph or growth habit, are commonly found in contexts such as food science, pharmaceutical processing, biomineralization, and biological antifreeze agents.[30] However, efforts to understand and exploit soluble additives during growth of organic semiconductor crystals remain in their early stages. Since the interactions between π-conjugated systems often dominate the crystallization behavior of these materials, we suspect that the ability to modify crystal growth of one conjugated organic material with another should be a rather general phenomenon. Indeed, it seems likely that such effects may have played a role in numerous previous studies on the formation of device layers from mixtures of p- and n-type conjugated molecules, although their importance was not necessarily appreciated at the time.

Notably, the previous studies in which conjugated polymers were intentionally used to modify the growth of small molecule organic semiconductor crystals have relied simply on solvent evaporation to induce crystallization.[26–29] This provides little control over the kinetics of crystal nucleation and growth and yields sensitivity to the details of the solvent removal process. The resulting nanostructures therefore show poorly controlled and broadly distributed sizes, which is a complicating factor both for fundamental studies of their photophysical properties as well as for fabrication of uniform device layers. A potential route to address this shortcoming is the use of sonocrystallization, which is routinely applied to control nucleation and growth of crystals of food ingredients, biomolecules, pharmaceuticals, and inorganic materials,[31,32] but has so far been used only in a few examples with organic semiconductors.[16,33–36] Though the mechanisms underlying sonocrystallization remain incompletely understood, the acoustic cavitation bubbles generated during application of ultrasound yield high temperatures, pressures, and shock waves that are thought to overcome the activation energy for crystal nucleation, enhance mass transport, and break up large crystals.[37–39] Generally, several effects of ultrasound on crystallization are found: a reduction in the supersaturation and time necessary for nucleation, and the growth of more uniformly sized crystals.

In the current report, we describe how the combined effects of P3HT to modify crystal growth, and ultrasound to facilitate nucleation, yield a simple route to suspensions of crystalline PDI nanowires with well-controlled dimensions and excellent colloidal stability. We consider the effects of P3HT/PDI ratio, P3HT molecular weight, and sonication temperature, and show that PDI nanowire widths can easily be tuned down to 14 nm, with polydispersities in width as small as 1.05. Further, we show how PDI nanocrystal seeds can be used for "living crystallization" of PDI, enabling formation of nanowires with well-controlled lengths and branched architectures.

RESULTS AND DISCUSSION

We begin by considering the behavior of supersaturated solutions of *N*,*N*′-dioctyl perylene diimide (PDI) in 1,2-dichlorobenzene (*o*DCB) containing P3HT (M_W = 20 kg/mol, regioregularity >98%), as summarized in Figure 1. Solutions with PDI concentrations of 1.5 mg/mL, well in excess of the room temperature solubility of 0.12 mg/mL previously estimated[26] from the amount of dissolved PDI remaining following quiescent crystallization for 26 days, are prepared by first heating to 80 °C and subsequently cooling to 25 °C. Unlike solutions of PDI alone, which recrystallize into micrometer-scale crystals over 10–20 min, the

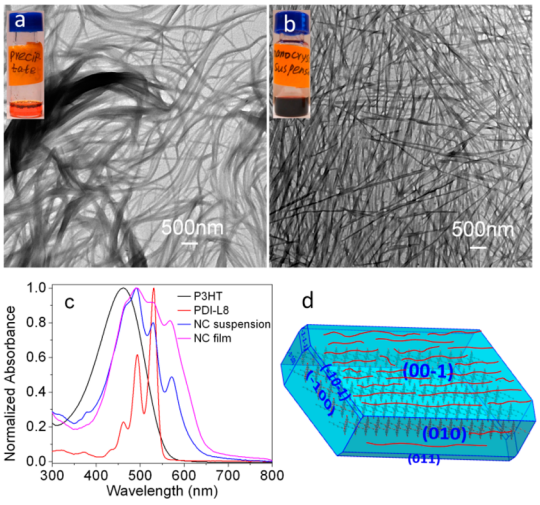

Figure 1. Crystals grown from a supersaturated solution containing 1.5 mg/mL of PDI and 1.0 mg/mL of P3HT (a) without, and (b) with insonation at 20 °C for 2 h. The insets are photographs of the corresponding suspensions after storage at room temperature for several months. (c) UV−vis absorption spectra of metastable solutions containing 1.0 mg/mL P3HT alone, 1.5 mg/mL PDI alone, and a blend of the two after insonation in the suspension state (NC suspension) and a dried film (NC film). (d) A schematic illustration showing the adsorption of P3HT chains (red lines) preferentially on the 010 and 001 faces of PDI nanocrystals.

presence of P3HT in solution, for example, at 1.0 mg/mL, yields a kinetically stabilized supersaturated solution. After ~4 h, however, flocculated PDI crystals floating at the air interface are visible, and within roughly 2 weeks, the concentration of dissolved PDI reaches the steady-state value of 0.12 mg/mL. The resulting PDI crystals have a broad distribution of sizes, as shown in Figure 1a for respective P3HT and PDI concentrations of 1.0 and 1.5 mg/mL.

In stark contrast to these results, when ultrasound is applied to supersaturated solutions containing P3HT, a visual color change indicative of crystallization is observed after 2 min and PDI crystal growth is completed within ~2 h. Furthermore, the resulting nanowire crystals, shown in Figure 1b, exhibit much narrower (mean: 38 nm) and more tightly distributed widths (polydispersity: 1.20), while their lengths can be up to tens of micrometers. Compared to the PDI crystals prepared without insonation (Figure 1a), these wires are also straighter and less agglomerated. The relatively well-controlled sizes of these fibers allow for the preparation of nearly smooth films (Supporting Information Figure S1), as evidenced by the decreased root-mean-square roughness, which is essential for achieving good contact between active layers and electrodes in high performance electronic devices. X-ray diffraction data (Supporting Information Figure S2) reveal that the crystalline structure of the nanowires formed by sonication remains the same as that of those formed without sonication and in the absence of P3HT. UV−vis spectroscopy (Figure 1c) shows that, in addition to the relatively sharp peaks characteristic of dissolved PDI, and the broad peak due to dissolved and adsorbed P3HT, a new sharp peak emerges at 572 nm following insonation, due to the formation of PDI crystals.[40] Notably, the absorption spectra of the sonicated nanowire suspension and a solid film cast from suspension are very similar, consistent with the nearly complete crystallization of PDI induced by ultrasound. (Some broadening of the absorption peaks and an increase in intensity of the red-shifted peaks is seen for the solid film, although this likely also reflects the crystallization of dissolved P3HT upon solvent evaporation.)

The BFDH (Bravais, Friedel, Donnay and Harker) prediction for the PDI crystal morphology based on the previously established single crystal structure[21] is shown in Figure 1d. In light of the high aspect ratios of the nanowires in Figure 1b, it appears that P3HT adsorbs preferentially to the (001) and (010) faces relative to the (100) faces, thus slowing crystal growth in the lateral dimensions relative to that along the nanowire length. As PDI crystals have been reported to be highly terraced,[41] it is also possible that P3HT adsorption occurs at step edges along these crystal faces. While the detailed nature of the interaction between P3HT and PDI crystals remains an important topic for future study, we suspect that $\pi-\pi$ interactions between the respectively electron rich and electron poor π-systems of P3HT and PDI likely represent a substantial contribution. Notably, the nanowires remain stable and homogeneously suspended in *o*DCB for at least 1 year, without any clear change in fiber width or agglomeration, suggesting their potential suitability as nanoscale "inks" for large-scale solution processing of organic electronic devices.

Further insight into the mechanism of P3HT-modified sonocrystallization is provided by several additional experiments described in more detail in the Supporting Information. First, emulsion crystallization measurements performed by first heating droplets of a supersaturated solution of PDI in *o*DCB to 80 °C and cooling at a rate of 2 °C/min reveal that only a small fraction of droplets—*i.e.*, those containing heterogeneous nucleation sites—undergo crystallization by 25 °C (Supporting Information Figure S3), while most of the remaining droplets undergo crystallization at 5 °C, consistent with homogeneous nucleation. Emulsions cooled to 25 °C and stored at room temperature show no additional crystallization for at least 4 h. This indicates that formation of PDI crystals at room temperature occurs almost exclusively by heterogeneous nucleation, and that homogeneous nucleation in quiescent solution can therefore be ignored on the time-scales of interest. With P3HT, no heterogeneously nucleated PDI crystals are observed at 25 °C, and homogeneous crystallization is postponed to −3 °C. Interpreted solely in terms of nucleation, this suggests

that P3HT serves to both poison heterogeneous nucleation sites and inhibit homogeneous nucleation of PDI crystals. However, P3HT may also slow the overall crystal growth rate, making it difficult to unambiguously identify its effect on nucleation compared to growth.

On the basis of these observations, we propose the following mechanism for the formation of stable PDI nanowire suspensions by sonocrystallization with P3HT. First, sonication greatly facilitates homogeneous nucleation of PDI crystals, leading to rapid formation of large numbers of crystal nuclei. After PDI nuclei form, P3HT preferentially adsorbs on the (001) and (010) crystal faces, which leads to faster PDI crystal growth along the nanowire axis compared to the lateral directions, yielding thin and narrow PDI nanowires. The overall crystallization rate may be enhanced by ultrasound not only due to the increased nucleation rate, but also due to better mixing by acoustic streaming, or by stripping P3HT chains off of PDI crystal faces.

We next consider the effect of varying P3HT concentration on sonocrystallization with a fixed PDI concentration of 1.5 mg/mL. Since PDI reaches almost full crystallinity through this process, we take the crystal dimensions measured from TEM images (Figure 2a–d) for samples simply dropcast on TEM grids as representative of the dimensions in suspension. We note, however, that small increases in nanowire size likely occur as the remaining 4–12% of soluble PDI crystallizes during solvent evaporation. The average width of PDI nanocrystals, determined by measurements of 300–500 crystals from TEM images, decreases from 200 to 40 nm upon increasing the P3HT concentration from 0.01 to 1 mg/mL, as seen in Figure 2e. By comparison, the average size of crystals grown when subjected to ultrasound in the absence of P3HT is 2.0 μm. The polydispersity of PDI fiber widths (defined as the width-average width divided by the number-average width) is also reduced from 1.4 to 1.2 over this range of P3HT concentration, presumably reflecting the slowing rate of crystal growth compared with nucleation as the P3HT concentration increases. Notably, it is also possible for ultrasound to induce crystallization of P3HT.[34−36] However, for mixtures with P3HT concentrations up to 1.0 mg/mL, we do not observe P3HT fibrils by TEM, which can be distinguished from PDI crystals due to their smaller widths of roughly 20 nm. Furthermore, X-ray diffraction data (Supporting Information Figure S2) show no evidence of crystalline P3HT under these conditions. Presumably, at these modest P3HT concentrations, adsorption to PDI nanocrystals lowers the concentration of free P3HT sufficiently to prevent crystallization.

At higher P3HT concentrations of 10–15 mg/mL, however, a shift in morphology to shish-kebab crystals[26] consisting of central PDI nanowires (widths of 20–15 nm, width polydispersities of 1.11–1.05)

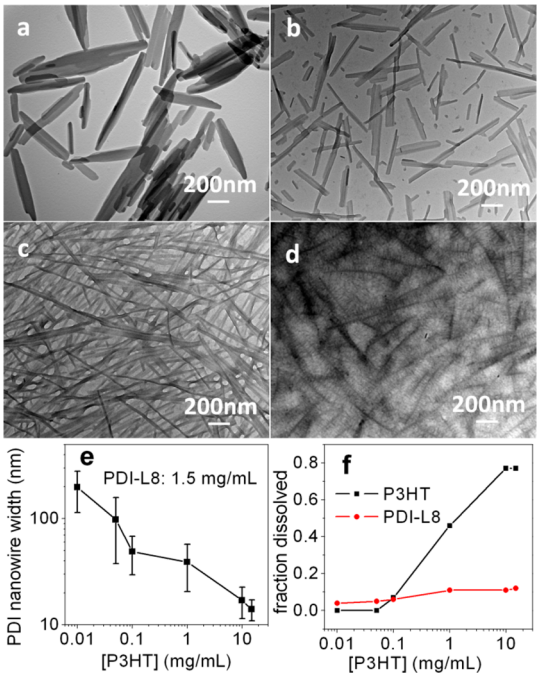

Figure 2. Sonocrystallized PDI-L8 nanocrystals formed at a concentration of 1.5 mg/mL with P3HT concentrations of (a) 0.01 mg/mL, (b) 0.1 mg/mL, (c) 1.0 mg/mL, (d) 15.0 mg/mL. (e) The width of PDI nanowires and (f) the fraction of remaining dissolved P3HT and PDI following insonation, as measured from ^{1}H NMR spectra, are plotted as a function of initial P3HT concentration.

flanked by P3HT fibrils are observed (*e.g.*, Figure 2d), indicating that the PDI nanowires serve to nucleate crystals of excess P3HT in solution as solvent evaporates. Further increases in P3HT concentration above 15 mg/mL yield highly viscous suspensions due to the presence of high aspect ratio PDI nanowires as well as crystallization of P3HT into fibrils, which may be assisted by both the presence of PDI nanowires as nucleation sites and the application of ultrasound. The P3HT fibrils and PDI nanowires formed under these conditions had similar widths, thus making it difficult to distinguish them from each other and complicating quantitative measurements. While the widths of the PDI wires can be tuned and show reasonably narrow distributions, the length of nanowires so far remains poorly controlled, perhaps for several reasons. One possibility is that the longitudinal growth rate remains relatively fast compared to the nucleation rate. Another is that ultrasound may break the wires as they grow, broadening the dispersity in length.

To determine the fractions of both PDI and P3HT remaining in solution following sonocrystallization, we perform solution state ^{1}H NMR measurements on supersaturated solutions containing 1.5 mg/mL of PDI both before and after sonication, as summarized in Figure 2f. At low P3HT concentrations, *e.g.* 0.01 mg/mL, only 4.4% (0.066 mg/mL) of the original PDI concentration remains dissolved in solution after insonation (assessed using the intensity of the peak at δ = 4.07 ppm,

Supporting Information Figure S4). This value is lower than the solubility of 0.12 mg/mL estimated from quiescent crystallization, indicating that ultrasound serves to reduce PDI supersolubility.[42] With increasing P3HT concentration, the remaining soluble fraction climbs to 10−12% (0.15−0.18 mg/mL), possibly reflecting an increase in PDI solubility as the crystal size decreases,[43] or a kinetic limitation on reaching the equilibrium solubility. The remaining dissolved P3HT concentration (from the peak at $\delta = 2.65$ ppm) drops to almost 0% at low initial P3HT concentrations, consistent with a high affinity binding of the polymer chains to the PDI crystal surfaces, but then climbs to ~80% at the highest P3HT concentrations studied. Unfortunately, further quantitative analysis of these data is complicated by the possibility for P3HT to disappear from solution also by crystallizing on its own at concentrations above 1 mg/mL. At lower concentrations, however, the data are reasonably consistent with nearly complete adsorption of P3HT chains on PDI crystal surfaces, as judged from a rough comparison of the total surface area of PDI crystals and the amount of available P3HT. For example, at a concentration of P3HT = 0.1 mg/mL, we estimate a total PDI crystal surface area per volume of suspension of 140 m^2/L, by treating the PDI crystals as rectangular in cross section with a constant width to thickness ratio of 2 (estimated from AFM measurements), ignoring the nanowire ends, and using a literature density value of 1.2 g/cm^3 for PDI crystals.[21] From ^{1}H NMR, the amount of P3HT removed from solution is 0.093 mg/mL, which together with the literature dimensions of a hexyl thiophene unit of 0.39 nm × 1.6 nm[44] yields an estimate of the total P3HT area per volume of 210 m^2/L, which is in reasonable agreement with the estimated PDI crystal surface area. Thus, we suggest that at low concentrations, P3HT almost completely absorbs to form a nearly complete monolayer on the PDI crystal surfaces.

On the basis of the proposed mechanism, we expect that P3HT molecular weight should have a pronounced effect on the dimensions of PDI nanocrystals. Higher molecular weights should provide stronger binding of P3HT chains, with slower desorption kinetics, and therefore reduced lateral crystal dimensions. Indeed, as shown in Figure 3a,b, compared with an average width of 39 nm for PDI fibers sonocrystallized at room temperature with 20 kg/mol P3HT (respective concentrations of 1.0 and 1.5 mg/mL), the PDI crystals increase dramatically to 150−500 nm in width using 6 kg/mol P3HT, and decrease to 25 nm in width using 60 kg/mol P3HT. Temperature provides another means to modulate crystal dimensions, although since nucleation, growth, and adsorption/desorption rates are all temperature-dependent, the net effect is not as easily anticipated. In practice, however, we find an increase in width to 70−200 nm when sonocrystallization is conducted at 40 ± 2 °C, and a decrease in width to 21 nm at 3 ± 1 °C.

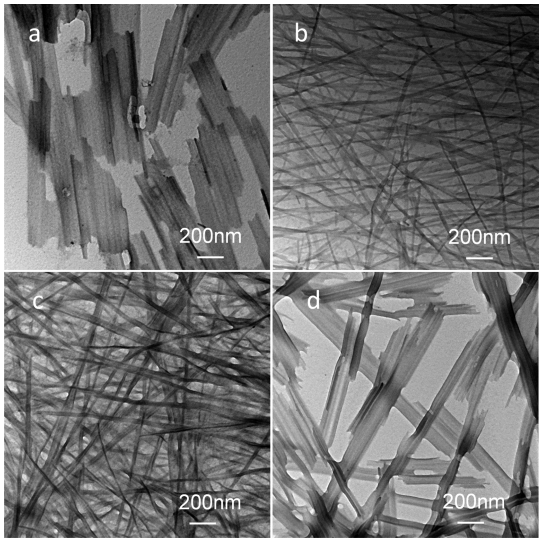

Figure 3. PDI nanocrystals sonocrystallized from solutions containing 1.5 mg/mL of PDI and 1.0 mg/mL of P3HT (a and b) at 20 °C with different P3HT molecular weights: (a) M_W = 6 kg/mol, (b) M_W = 60 kg/mol), and (c and d) with M_W = 20 kg/mol at temperatures of (c) 3 ± 1 °C, (d) 40 ± 2 °C.

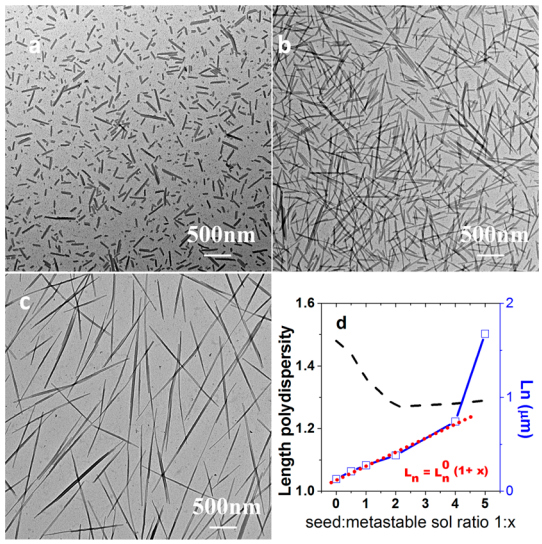

Figure 4. (a) Seed crystals of PDI prepared by sonocrystallization of solutions containing 1.0 mg/mL P3HT and 2.0 mg/mL PDI at 20 °C for 9 h; (b and c) are extended by mixing with metastable solutions of the same P3HT/PDI concentrations at volumetric ratios of (b) 1:2 and (c) 1:5. (d) A plot of the number-average length L_n (blue curve) and length polydispersity (black dashed curve) as a function of the seed/metastable solution mixing ratio 1:x. The dotted red line represents the expected dependence for extension of seeds by living crystallization.

The uniformity of the sonocrystallized PDI naonowires suggests the possibility to use them as seeds to induce further growth of PDI, in similar fashion to the approach of "living crystallization" developed by Manners, Winnik, and co-workers.[45,46] To prepare seed crystals, we extended the length of sonication to 9 h

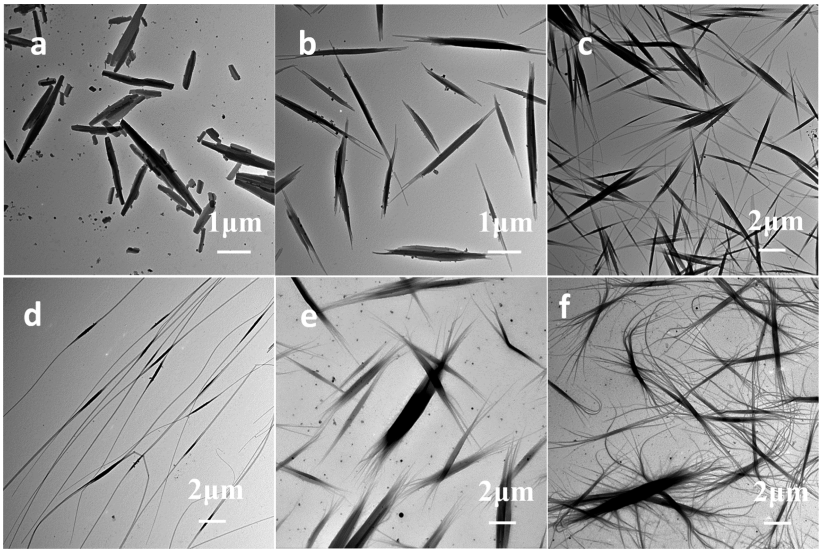

Figure 5. Wide PDI seeds formed by sonocrystallization with a P3HT concentration of 0.01 mg/mL and a PDI concentration of 1.5 mg/mL at 0 °C for 2 h (a). Extended crystals are obtained by adding metastable solutions of P3HT/PDI with different P3HT concentrations and a fixed PDI concentration of 1.5 mg/mL; solution/seed ratios of (b) 1:1, (c) 3:2, and (d) 3:1 with 0.1 mg/mL P3HT, and (e) 1:1, (f) 3:1 with 10 mg/mL P3HT.

(using respective P3HT and PDI concentrations of 1.0 and 2.0 mg/mL), which yields PDI crystals with number-average width and length of 34 and 129 nm, respectively, as shown in Figure 4a. Upon adding the seed suspension to metastable solutions of the same P3HT/PDI concentrations with a volumetric ratio of 1:*x*, the widths of the seeded grown PDI fibers stay at 34 ± 2 nm, while the lengths grow larger with increasing *x*. Representative TEM images of nanowires grown with $x = 2$ and 5 are shown in Figure 4, panels b and c, respectively. As shown in Figure 4d, for values of *x* up to 4, the number-average length follows very closely the relationship $L_n = L_n^0(1 + x)$ expected for living crystallization, in which every seed crystal is extended at a constant rate, with no termination or combination (here, L_n^0 is the average length of the seeds). Correspondingly, the length polydispersity (defined as the length-average length divided by the number-average length) decreases from 1.48 for the seeds, to 1.27 at $x = 2$. By $x = 5$, however, a population of very long PDI nanowires begins to form, which we suspect may come from the merging of shorter wires based on the presence of thin segments along individual long wires. Correspondingly, the plot of average length *vs x* shows a positive deviation from the linear trend, and a slight increase in length polydispersity. While the reasons for this loss of controlled crystallization are not completely clear at present, we suspect they occur due to a dramatic increase in viscosity of the suspension; indeed, further increases of *x* above 8 yield highly viscous gel-like materials following sonocrystallization.

The ability to extend seed crystals in a controlled fashion also offers access to branched nanowire structures, which we demonstrate using wide PDI seed crystals prepared at low P3HT concentrations (0.01 mg/mL P3HT, 1.5 mg/mL PDI) as shown in Figure 5a. With the use of metastable solutions with higher P3HT concentration and same PDI concentration for crystal extension, the ends of these wide seeds can serve to nucleate thinner PDI crystals. Figure 5b–d shows crystals extended at 0.1 mg/mL P3HT, where slightly thinner crystals grow from both ends of the original large crystals. With addition of increasing amounts of the metastable solution, the thinner crystals grow longer. For example when the mixed volume ratio of seed to metastable solution goes from 1:1 (Figure 5b) to 2:3 (Figure 5c), the lengths of the thinner regions increase from 1 ± 0.5 to 4 ± 2 μm. Notably, as the mixing ratio of seeds to metastable solution reaches 1:3, macroscopic gel-like clumps of highly aggregated segmented PDI crystals grown from micrometer-sized seeds are formed (as determined by TEM). However, above this aggregated material, narrower segmented PDI crystals (Figure 5d) grown from 120 ± 30 nm wide seeds are found in a thin layer of supernatant. When the seeds are instead extended with much narrower nanowires at 10 mg/mL P3HT (Figure 5e,f), they form highly branched crystals that can be further extended by increasing the quantity of metastable solution added. We note that similar types of branched crystalline nanowires have been demonstrated for poly(ferrocenylsilane)-based block copolymers, although in that case crystal width was adjusted through variation of the block ratios, rather than concentration of an adsorbing additive.[45]

CONCLUSION

In conclusion, we have shown that sonocrystallization of a perylene diimide derivative using poly(3-hexyl thiophene) as a soluble crystal modifier provides a

powerful means to tailor the dimensions and morphology of crystalline nanowires of a conjugated small molecule. Ultrasound appears to dramatically increase the rate of crystal nucleation; coupled with the adsorption of P3HT to the crystal surfaces, this leads to the formation of nanowires with well-defined and tunable lateral dimensions. In addition to the ratio of P3HT to PDI concentrations, P3HT molecular weight and sonication temperature provide handles to control the process. Using well-controlled PDI crystals as seeds, we have further demonstrated the controlled extension through "living crystallization" to yield nanowires with reduced length polydispersity, as well as branched crystals. We anticipate that similar effects may be found in other combinations of conjugated polymers and small molecules, and that the method may therefore provide an easily scalable approach to prepare nanocrystalline building blocks for the fabrication of organic electronics.

EXPERIMENTAL SECTION

Materials. P3HT with weight-average molecular weights of 20 and 60 kg/mol were purchased from Rieke Metals, while that of 6 kg/mol was synthesized according to literature procedures.[47] PDI and *o*DCB were purchased from Sigma-Aldrich. All purchased materials were used as received.

Nanocrystal Suspension Preparation. Desired masses of P3HT and PDI were dissolved by heating in *o*DCB at 120 °C for 10 min in the dark. After complete dissolution, solutions were filtered with a 0.45 μm PTFE filter. The blend solution was then exposed to ultrasound using a 35 kHz VWR Symphony ultrasonic cleaner at the indicated temperature, maintained by an ice−water bath or hot water bath. The solution was shaken by hand for 0.5 h and then subjected to ultrasound for another 1.5 h without agitation. TEM samples were prepared by dropcasting volumes of less than 1 μL of the suspensions on TEM grids, and then removing excess liquid with filter paper.

Emulsion Crystallization. PDI emulsions with or without P3HT were prepared by emulsifying *o*DCB solutions in twice the volume of an aqueous phase containing 5 mg/mL poly(vinyl alcohol) (PVOH, 13−23 kg/mol, 98% hydrolyzed, Aldrich) with vortex mixing for several minutes. Emulsions were then loaded into 50 μm thick optical capillaries and open ends were sealed with epoxy prior to observing under an optical microscope.

Measuring Remaining Dissolved P3HT and PDI Concentrations. We use the residual proton signal at 6.71 ppm from 1,2-dichlorobenzene-d_4 (98% deuterated, Aldrich) as an internal standard for ^{1}H NMR measurements. The integrated intensities of the peaks at 2.65 ppm for P3HT, and at 4.07 ppm for PDI measured from an Agilent 700 MHz NMR spectrometer, along with the known concentrations of the samples prior to insonation, were then used to determine the absolute dissolved concentrations of both species following ultrasound.

Seeded Growth. Suspensions of seed crystals were added to metastable solutions in the desired volume ratio, followed by gentle shaking to mix. The samples were then kept quiescent in the dark for at least 24 h before TEM sample preparation. Lengths are characterized in terms of

$$\text{number average length, } L_n = \frac{\sum_{i=1}^{i=n} N_i L_i}{\sum_{i=1}^{i=n} N_i}$$

$$\text{length average length, } L_l = \frac{\sum_{i=1}^{i=n} N_i L_i^2}{\sum_{i=1}^{i=n} N_i L_i}$$

$$\text{and length polydispersity} = \frac{L_l}{L_n}$$

Conflict of Interest: The authors declare no competing financial interest.

Supporting Information Available: AFM and OM images, XRD and ^{1}H NMR of P3HT/PDI nanocrystals. This material is available free of charge *via* the Internet at http://pubs.acs.org.

Acknowledgment. This work was supported by the Department of Energy, Basic Energy Sciences, through grant DE-SC0006639 (all work described) and made use of facilities supported by the National Science Foundation MRSEC at UMass (DMR-0820506). T.J.D. was supported by the National Science Foundation through the CURE REU Program at UMass (CHE-1004983).

REFERENCES AND NOTES

1. Heeger, A. J. 25th Anniversary Article: Bulk Heterojunction Solar Cells: Understanding the Mechanism of Operation. *Adv. Mater.* **2013**, *26*, 10–28.
2. Noriega, R.; Rivnay, J.; Vandewal, K.; Koch, F. P. V.; Stingelin, N.; Smith, P.; Toney, M. F.; Salleo, A. A General Relationship between Disorder, Aggregation and Charge Transport in Conjugated Polymers. *Nat. Mater.* **2013**, *12*, 1037–1043.
3. Li, R. J.; Hu, W. P.; Liu, Y. Q.; Zhu, D. B. Micro- and Nanocrystals of Organic Semiconductors. *Acc. Chem. Res.* **2010**, *43*, 529–540.
4. Liu, F.; Gu, Y.; Jung, J. W.; Jo, W. H.; Russell, T. P. On the Morphology of Polymer-Based Photovoltaics. *J. Polym. Sci., Part B: Polym. Phys.* **2012**, *50*, 1018–1044.
5. Liao, H. C.; Ho, C. C.; Chang, C. Y.; Jao, M. H.; Darling, S. B.; Su, W. F. Additives for Morphology Control in High-Efficiency Organic Solar Cells. *Mater. Today* **2013**, *16*, 326–336.
6. He, M.; Wang, M. Y.; Lin, C. J.; Lin, Z. Q. Optimization of Molecular Organization and Nanoscale Morphology for High Performance Low Bandgap Polymer Solar Cells. *Nanoscale* **2014**, *6*, 3984–3994.
7. Dang, M. T.; Hirsch, L.; Wantz, G.; Wuest, J. D. Controlling the Morphology and Performance of Bulk Heterojunctions in Solar Cells. Lessons Learned from the Benchmark Poly(3-hexylthiophene): 6,6-Phenyl-C-61-butyric Acid Methyl Ester System. *Chem. Rev.* **2013**, *113*, 3734–3765.
8. Arias, A. C.; MacKenzie, J. D.; McCulloch, I.; Rivnay, J.; Salleo, A. Materials and Applications for Large Area Electronics: Solution-Based Approaches. *Chem. Rev.* **2010**, *110*, 3–24.
9. Samitsu, S.; Shimomura, T.; Ito, K. Nanofiber Preparation by Whisker Method Using Solvent-Soluble Conducting Polymers. *Thin Solid Films* **2008**, *516*, 2478–2486.
10. Kim, F. S.; Ren, G. Q.; Jenekhe, S. A. One-Dimensional Nanostructures of π-Conjugated Molecular Systems: Assembly, Properties, and Applications from Photovoltaics, Sensors, and Nanophotonics to Nanoelectronics. *Chem. Mater.* **2011**, *23*, 682–732.
11. Berson, S.; De Bettignies, R.; Bailly, S.; Guillerez, S. Poly(3-hexylthiophene) Fibers for Photovoltaic Applications. *Adv. Funct. Mater.* **2007**, *17*, 1377–1384.
12. Xin, H.; Kim, F. S.; Jenekhe, S. A. Highly Efficient Solar Cells based on Poly(3-butylthiophene) Nanowires. *J. Am. Chem. Soc.* **2008**, *130*, 5424–5425.
13. Li, L. G.; Lu, G. H.; Yang, X. N. Improving Performance of Polymer Photovoltaic Devices Using an Annealing-Free

Approach *via* Construction of Ordered Aggregates in Solution. *J. Mater. Chem.* **2008**, *18*, 1984–1990.
14. Yu, W.; Yang, D.; Zhu, X. G.; Wang, X. L.; Tu, G. L.; Fan, D. Y.; Zhang, J.; Li, C. Control of Nanomorphology in All-Polymer Solar Cells *via* Assembling Nanoaggregation in a Mixed Solution. *ACS Appl. Mater. Interfaces* **2014**, *6*, 2348–2353.
15. Bag, M.; Gehan, T. S.; Algaier, D. D.; Liu, F.; Nagarjuna, G.; Lahti, P. M.; Russell, T. P.; Venkataraman, D. Efficient Charge Transport in Assemblies of Surfactant-Stabilized Semiconducting Nanoparticles. *Adv. Mater.* **2013**, *25*, 6411–6415.
16. Nagarjuna, G.; Baghgar, M.; Labastide, J. A.; Algaier, D. D.; Barnes, M. D.; Venkataraman, D. Tuning Aggregation of Poly(3-hexylthiophene) within Nanoparticles. *ACS Nano* **2012**, *6*, 10750–10758.
17. Liu, J. S.; Sheina, E.; Kowalewski, T.; McCullough, R. D. Tuning the Electrical Conductivity and Self-Assembly of Regioregular Polythiophene by Block Copolymerization: Nanowire Morphologies in New Di- and Triblock Copolymers. *Angew. Chem., Int. Ed.* **2002**, *41*, 329–332.
18. Wang, H. W.; Pentzer, E.; Emrick, T.; Russell, T. P. Preparation of Low Band Gap Fibrillar Structures by Solvent-Induced Crystallization. *ACS Macro Lett.* **2014**, *3*, 30–34.
19. Hahm, S. G.; Rho, Y.; Jung, J.; Kim, S. H.; Sajoto, T.; Kim, F. S.; Barlow, S.; Park, C. E.; Jenekhe, S. A.; Marder, S. R.; et al. High-Performance n-Channel Thin-Film Field-Effect Transistors Based on a Nanowire-Forming Polymer. *Adv. Funct. Mater.* **2013**, *23*, 2060–2071.
20. Ren, G. Q.; Ahmed, E.; Jenekhe, S. A. Nanowires of Oligothiophene-Functionalized Naphthalene Diimides: Self Assembly, Morphology, and All-Nanowire Bulk Heterojunction Solar Cells. *J. Mater. Chem.* **2012**, *22*, 24373–24379.
21. Briseno, A. L.; Mannsfeld, S. C. B.; Reese, C.; Hancock, J. M.; Xiong, Y.; Jenekhe, S. A.; Bao, Z.; Xia, Y. N. Perylenediimide Nanowires and Their Use in Fabricating Field-Effect Transistors and Complementary Inverters. *Nano Lett.* **2007**, *7*, 2847–2853.
22. Zang, L.; Che, Y. K.; Moore, J. S. One-Dimensional Self-Assembly of Planar pi-Conjugated Molecules: Adaptable Building Blocks for Organic Nanodevices. *Acc. Chem. Res.* **2008**, *41*, 1596–1608.
23. Lim, J. A.; Lee, H. S.; Lee, W. H.; Cho, K. Control of the Morphology and Structural Development of Solution-Processed Functionalized Acenes for High-Performance Organic Transistors. *Adv. Funct. Mater.* **2009**, *19*, 1515–1525.
24. Cao, X. Q.; Wu, Y. S.; Fu, H. B.; Yao, J. N. Self-Assembly of Perylenediimide Nanobelts and Their Size-Tunable Exciton Dynamic Properties. *J. Phys. Chem. Lett.* **2011**, *2*, 2163–2167.
25. Hartnett, P. E.; Timalsina, A.; Matte, H. S. S. R.; Zhou, N.; Guo, X.; Zhao, W.; Facchetti, A.; Chang, R. P. H.; Hersam, M. C.; Wasielewski, M. R.; et al. Slip-Stacked Perylenediimides as an Alternative Strategy for High Efficiency Nonfullerene Acceptors in Organic Photovoltaics. *J. Am. Chem. Soc.* **2014**, *136*, 16345–16356.
26. Bu, L. J.; Pentzer, E.; Bokel, F. A.; Emrick, T.; Hayward, R. C. Growth of Polythiophene/Perylene Tetracarboxydiimide Donor/Acceptor Shish-Kebab Nanostructures by Coupled Crystal Modification. *ACS Nano* **2012**, *6*, 10924–10929.
27. Li, L.; Jacobs, D. L.; Bunes, B. R.; Huang, H.; Yang, X.; Zang, L. Anomalous High Photovoltages Observed in Shish Kebab-like Organic p−n Junction Nanostructures. *Polym. Chem.* **2014**, *5*, 309–313.
28. Chen, J. H.; Shao, M.; Xiao, K.; He, Z. R.; Li, D. W.; Lokitz, B. S.; Hensley, D. K.; Kilbey, S. M.; Anthony, J. E.; Keum, J. K.; et al. Conjugated Polymer-Mediated Polymorphism of a High Performance, Small-Molecule Organic Semiconductor with Tuned Intermolecular Interactions, Enhanced Long-Range Order, and Charge Transport. *Chem. Mater.* **2013**, *25*, 4378–4386.
29. Suzuki, T.; Okamoto, T.; Saeki, A.; Seki, S.; Sato, H.; Matsuo, Y. Formation of Photoconductive Nanowires of Tetracene Derivative in Composite Thin Film. *ACS Appl. Mater. Interfaces* **2013**, *5*, 1937–1942.
30. Song, R. Q.; Cölfen, H. Additive Controlled Crystallization. *CrystEngComm* **2011**, *13*, 1249–1276.
31. Ruecroft, G.; Hipkiss, D.; Ly, T.; Maxted, N.; Cains, P. W. Sonocrystallization: The Use of Ultrasound for Improved Industrial Crystallization. *Org. Process Res. Dev.* **2005**, *9*, 923–932.
32. Li, H.; Wang, J. K.; Bao, Y.; Guo, Z. C.; Zhang, M. Y. Rapid Sonocrystallization in the Salting-out Process. *J. Cryst. Growth* **2003**, *247*, 192–198.
33. Kang, P.; Chen, C. N.; Hao, L. Y.; Zhu, C. L.; Hu, Y.; Chen, Z. Y. A Novel Sonication Route To Prepare Anthracene Nanoparticles. *Mater. Res. Bull.* **2004**, *39*, 545–551.
34. Zhao, K.; Xue, L. J.; Liu, J. G.; Gao, X.; Wu, S. P.; Han, Y. C.; Geng, Y. H. A New Method To Improve Poly(3-hexyl thiophene) (P3HT) Crystalline Behavior: Decreasing Chains Entanglement To Promote Order-Disorder Transformation in Solution. *Langmuir* **2010**, *26*, 471–477.
35. Kim, B. G.; Kim, M. S.; Kim, J. Ultrasonic-Assisted Nanodimensional Self-Assembly of Poly-3-hexylthiophene for Organic Photovoltaic Cells. *ACS Nano* **2010**, *4*, 2160–2166.
36. Aiyar, A. R.; Hong, J. I.; Izumi, J.; Choi, D.; Kleinhenz, N.; Reichmanis, E. Ultrasound-Induced Ordering in Poly(3-hexylthiophene): Role of Molecular and Process Parameters on Morphology and Charge Transport. *ACS Appl. Mater. Interfaces* **2013**, *5*, 2368–2377.
37. Sehgal, C.; Steer, R. P.; Sutherland, R. G.; Verrall, R. E. Sonoluminescence of Argon Saturated Alkali-Metal Salt-Solutions as a Probe of Acoustic Cavitation. *J. Chem. Phys.* **1979**, *70*, 2242–2248.
38. de Castro, M. D. L.; Priego-Capote, F. Ultrasound-Assisted Crystallization (Sonocrystallization). *Ultrason. Sonochem.* **2007**, *14*, 717–724.
39. Cravotto, G.; Gaudino, E. C.; Cintas, P. On the Mechanochemical Activation by Ultrasound. *Chem. Soc. Rev.* **2013**, *42*, 7521–7534.
40. Balakrishnan, K.; Datar, A.; Oitker, R.; Chen, H.; Zuo, J. M.; Zang, L. Nanobelt Self-Assembly from an Organic n-Type Semiconductor: Propoxyethyl-PTCDI. *J. Am. Chem. Soc.* **2005**, *127*, 10496–10497.
41. Usowicz, M. T.; Kelley, M. J.; Singer, K. D.; Duzhko, V. V. Tailored One- and Two-Dimensional Self-Assembly of a Perylene Diimide Derivative in Organic Solvents. *J. Phys. Chem. B* **2011**, *115*, 9703–9709.
42. Van Hook, A. *Crystallization: Theory and Practice*; Reinhold Pub. Corp.: New York, 1961.
43. Hulett, G. A. The Solubility of Gypsum As Affected by Size of Particles and by Different Crystallographic Surfaces. *J. Am. Chem. Soc.* **1905**, *27*, 49–56.
44. Brinkmann, M. Structure and Morphology Control in Thin Films of Regioregular Poly(3-hexylthiophene). *J. Polym. Sci., Part B: Polym. Phys.* **2011**, *49*, 1218–1233.
45. Gädt, T.; Ieong, N. S.; Cambridge, G.; Winnik, M. A.; Manners, I. Complex and Hierarchical Micelle Architectures from Diblock Copolymers Using Living, Crystallization-Driven Polymerizations. *Nat. Mater.* **2009**, *8*, 144–150.
46. Gwyther, J.; Gilroy, J. B.; Rupar, P. A.; Lunn, D. J.; Kynaston, E.; Patra, S. K.; Whittell, G. R.; Winnik, M. A.; Manners, I. Dimensional Control of Block Copolymer Nanofibers with a Conjugated Core: Crystallization-Driven Solution Self-Assembly of Amphiphilic Poly(3-hexylthiophene)-b-poly(2-vinylpyridine). *Chem.—Eur. J.* **2013**, *19*, 9186–9197.
47. Loewe, R. S.; Ewbank, P. C.; Liu, J. S.; Zhai, L.; McCullough, R. D. Regioregular, Head-to-Tail Coupled Poly(3-alkylthiophenes) Made Easy by the GRIM Method: Investigation of the Reaction and the Origin of Regioselectivity. *Macromolecules* **2001**, *34*, 4324–4333.